CONTACTLESS MEDIUM ACCURACY ABSOLUTE POSITION SENSOR

A. Bolognini[(1)], N. Scheidegger[(1)], V. Dvorak[(2)]

[(1)] RUAG Space, Schaffhauserstr. 580, 8052 Zürich, Switzerland, Email: alessio.bolognini@ruag.com
[(2)] Brno University of Technology, Antonínská 548/1, 601 90 Brno-střed, Czechia, Email: vojtech.dvorak@vutbr.cz

ABSTRACT

There are not many space-qualified contactless absolute position sensors with a measurement accuracy of a few tenths of a degree available on the market. Sensors used to control mechanisms that are operated over an extended lifetime (60 Mrevs) are usually based on optical encoders which are sensitive to radiation and mechanical alignment. Where the high resolution provided by those optical encoders is not required for a particular application, a more robust and cost-effective solution should be used. The position sensor qualified for the MetOp-SG 3MI Filter Wheel Mechanism (FWM) fills this gap: it provides medium accuracy while keeping the advantage of being contactless and thus essentially wear free. A magneto-resistive position sensor used for industrial applications has been enhanced to increase its robustness against environmental loads. This paper presents the sensor's working principle, its design and the modifications that were deemed necessary to enable the sensor's use in a demanding space application.

1. INTRODUCTION

1.1. Filter Wheel Subsystem Overview

The multi-viewing, multi-channel, multi-polarisation imager (3MI) is one of the instruments onboard the Meteorological Operational Second Generation (MetOp-SG) Satellite A. Its goal is to capture pictures of the solar radiation reflected by the Earth-atmosphere, at different viewing angles, spectral ranges and polarization directions for climate and global change studies. The Filter Wheel Subsystem (FWS) function is to accurately position, in space and time, a set of optical filters in the optical path of the 3MI channels. The FWS is composed by the Filter Wheel Assembly (FWA) and the Filter Wheel Controller (FWC). The FWA (Fig. 1) features a high precision mechanism that securely supports the Filter Wheel Disk (FWD) carrying the optical elements during launch and in-orbit operation for a lifetime of more than 57 Mrevs [1]. The FWC (Fig. 2) is the interface between Instrument Control Unit (ICU) and FWA. It has been carefully designed to perform different simultaneous tasks, including synchronising the FWD rotation with triggers received from ICU, processing the position sensor signals and ensuring safe and reliable functioning for the entire FWS. A key element for the FWS control is the position sensor which is further described in the subsequent chapters.

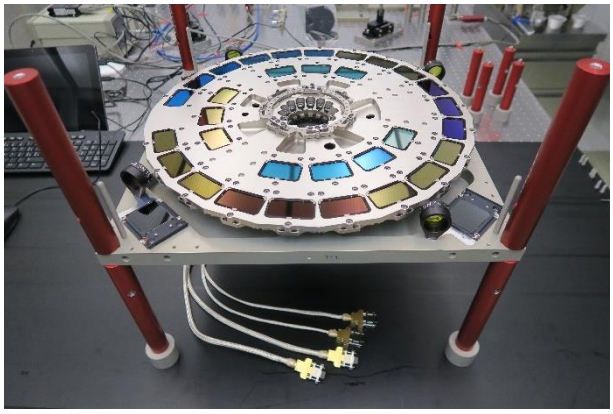

Figure 1. Filter Wheel Assembly (FWA)

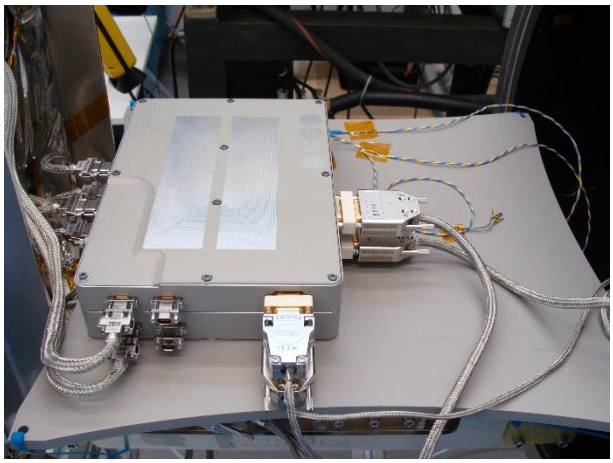

Figure 2. Filter Wheel Controller (FWC)

1.2. Position Sensors Working Principle

The absolute angular position sensor, installed in the FWA, is based on the Giant Magneto-Resistive (GMR) principle. The two main components are the sensor wheel and the reading head which are arranged as shown in Fig. 3. The sensor wheel, connected to the rotor, is made of ferromagnetic material and presents two precisely machined tracks with 75 (N1) and 74 (N2) teeth respectively. Every track is read by one pair of GMR sensors contained in each reading head. The reading head is composed by a total of four GMR sensing elements disposed in pairs and two Sm2Co17 permanent magnets generating the bias field. The rotation of the sensor wheel

leads to a variable magnetic field strength, due the variable distance of the track profile with respect to the position sensor, which is converted by the sensor elements into a sine and cosine signal for each track. The total output of each reading head is four differential sinusoidal signals: Sin_N1, Cos_N1, Sin_N2 and Cos_N2. The forementioned signals fulfil the Nonius principle (also called Vernier principle). They vary in amplitude, offset and phase characteristics in general. These sensor characteristics (rather than errors) are unique for each mechanism, depending on the properties of the reading heads and the assembly of sensor wheel into the mechanism. The four signals are then amplified, filtered, digitised and processed by the FWC to get the absolute position.

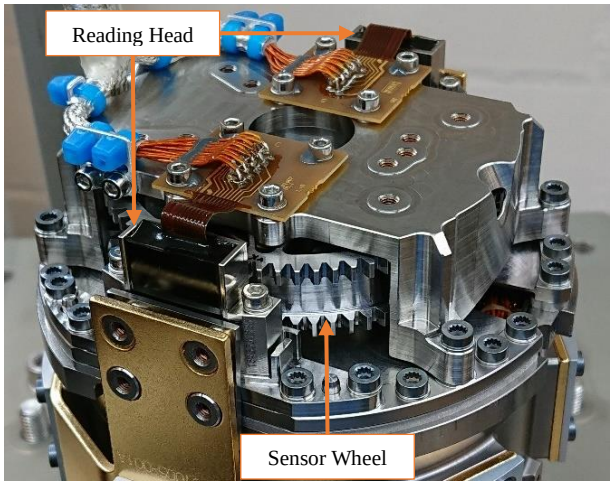

Figure 3. Filter Wheel Position Sensor

1.3. Position Estimation Chain

The differential signals generated by the position sensor are processed by FWC electronics. The signals are propagated through the Position Estimation Chain to estimate the current FWD position (Fig. 4).

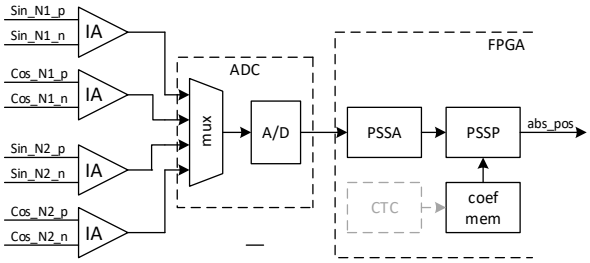

Figure 4. Scheme of Position Estimation Chain

First, single ended voltage signals are generated and amplified from differential signals by the Instrument Amplifiers (IA) with fixed gain and converted to the digital domain by A/D converter. There is one A/D converter paired to one analog multiplexer to acquire all four signals.

The digitised signals are acquired by the FPGA core. Due to the presence of the analog multiplexer, it is not possible to acquire all the samples at the same time. To compensate possible movement of position sensor wheel during one acquisition cycle, the sampling scheme shown in Fig. 5 is implemented in the acquisition core "Position Sensor Signals Acquisition" (PSSA). The acquisition core acquires two samples of each signal and performs linear interpolation of the two samples measured with fixed time steps. Such a symmetrical acquisition scheme ensures all interpolated values correspond to the values that would be acquired in the virtual centre of one acquisition cycle.

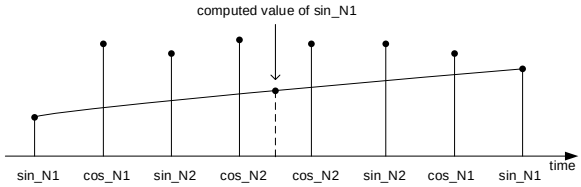

Figure 5. Acquisition schema of position sensor signals

The acquired set of data is propagated to a position estimation method, the "Position Sensor Signal Processing" (PSSP), to calculate the current position of the FWD. A new numerical method of position estimation was developed for this application. It provides better robustness and accuracy in case of drift of sensor characteristics with respect to common estimation methods. Further details on this algorithm are presented in chapter 2.

2. FWC POSITION ESTIMATION METHOD

2.1. Common Position Estimation Method

The usual methods to estimate position are exploiting the Nonius principle [2]. The common property of the methods is the sequence of correction of all sensor imperfections as listed below with differences in how to obtain phase in the current periods.

1. Correction of signal gain and offset characteristics.
2. Calculation of phase in the current period of signals on track N1 and track N2, either by goniometric function [3], e.g. according to equation (1) or utilizing observer phase-locked loop [4].
3. $$\varphi_{N1} = \operatorname{atan}\left(\frac{sin\_N1}{cos\_N1}\right)$$ $$\varphi_{N2} = \operatorname{atan}\left(\frac{sin\_N2}{cos\_N2}\right) \quad (1)$$
4. Application of Nonius principle: $$\varphi_{abs} = \varphi_{N1} - \varphi_{N2}$$
5. Compensation of phase characteristic as a last step.

The numerical method developed for FWS does not follow this common approach. It exploits the consequence of Vernier principle rather than the principle itself, that is, any angle of the position sensor is unique in terms of the combination of values of the position sensor output signals.

2.2. Novel Position Estimation Method

Assuming any position to be encoded into a set of values of sensor signals, a task to estimate position can be understood as a task to create a list of all valid combinations of sensor signals (sensor wheel model) and to define some function to evaluate similarities between the current samples of the sensor wheel and the model of the sensor wheel (Fig. 6).

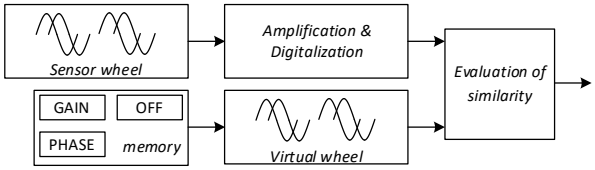

Figure 6. Concept of Novel Position Estimation Method

During position estimation, only the model of the sensor wheel (virtual wheel) is rotated and the digitised sensor signals are compared, in a purely numerical way, with virtual wheel values. The best match between the sensor samples and the virtual wheel corresponds to the absolute position of the virtual wheel. The advantage of this numerical method is that it does not require any correction of the input signals: imperfections, such as amplitude, offset and phase characteristics, are modelled on the fly during the virtual wheel generation.
Searching for the best match over the whole sensor model requires a lot of values of the virtual wheel to be evaluated thus requiring a high computational effort. Due to the numerical nature of this method, it is not always necessary to search over the whole revolution and the virtual wheel area can be reduced to a smaller size around the expected angle. These can be seen as different operational modes of the same method. While the *Exhaustive Mode* performs a full rotation of virtual wheel and search for the best match among all positions, *Fast Mode* performs a limited search around the last known position. Since there is an upper speed limit for the FWD, the search area and run period of the Fast Mode are set to correctly track position with high margin.
In chapter 2.3 and 2.4, the generation of virtual wheel and a method to evaluate similarity are respectively presented.

2.3. Virtual Wheel

There are a number of ways to assemble a model of the sensor wheel while considering different requirements such as accuracy of the model and necessary resources (i.e. computational effort, memory utilization and computation run time). The model with best accuracy (*ideal model*) describes the sensor signals on every position with exact values. The ideal model can be easily obtained after measuring all the values over a full revolution with required angular resolution. However, such model requires a lot of memory space to store all the values.
To overcome high memory utilization a *simplified model*, as an optimal trade-off between the requirements, was created. The simplified model splits the full revolution into number of sections of the same length, while each section is characterized by one set of coefficients (gain, offset, phase shift). While nearly infinite options are available to split the revolution, it was decided to follow the natural division of sensor wheel for FWS and each section is representing one tooth of sensor wheel. The number of sections is then N1 for signals sin_N1 and cos_N1 and N2 for sin_N2 and cos_N2.
The virtual wheel is generated on a given position φ_{vw} based on amplitude (G), offset (O) and phase shift (P) according to the equation (2). Equivalent equations can be defined also for the other signals.

$$sin\_N1_{vw}(\varphi_{vw}) = G(P_{N1}) * sin\,(N_1 * \varphi_{vw} + P(P_{N1})) + O(P_{N1}) \qquad (2)$$

The expected drawback of the simplified model is its inability to precisely emulate sensor signals because of the limited number of coefficients and introduction of discontinuities in the model at the edges of two consecutive periods, as reported in Fig. 7.

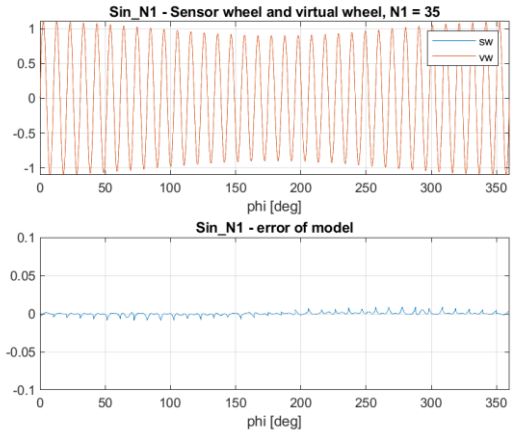

Figure 7. Virtual wheel of sin_N1 with model error

While there are some differences between the sensor wheel and the corresponding virtual wheel, it was found that with the presented method to find the best match, described in chapter 2.4, the error of the model is negligible and the position can be correctly estimated.

2.4. Evaluation Of Similarities

Given the sensor wheel model, a method to evaluate the similarities with respect to the virtual wheel can be defined.
The evaluation process consists of rotating the virtual wheel in the search area, according to the operational mode of the selected method, to generate all the values of virtual wheel. On every position of the virtual wheel (φ_{vw}), the generated values are compared with the digitised values of sensor signals. The comparison result is the curve representing a *differential function* δ. The exact shape of the curve depends on the definition function, actual parameters of the sensor signals and the inaccuracy of the virtual wheel. An example of the shape of a differential function is shown in Fig. 8. The most important property of the differential function is the existence of a global minimum. The angle of the virtual wheel, where the global minimum is located, is the absolute position of FWD.

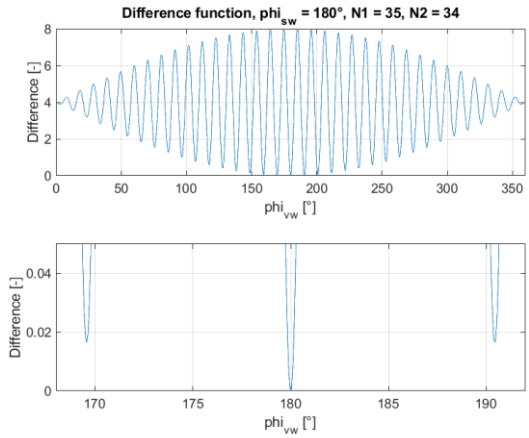

Figure 8. Differential function

3. FWM POSITION SENSOR DESIGN

3.1. Industrial Read Head Design

The read head key elements are shown in Fig. 9 and include two Magneto-Resistive (MR) sensors, each one consisting of two Wheatstone bridges offset by a quarter tooth pitch and made up of four GMR resistors, soldered on to the rigid part of a rigid-flex PCB, permanent magnets which are mounted on the top side of the rigid PCB and generate a biasing magnetic field through the sensors, and a housing which provide the structural support for these functional elements.
The read head functional elements are connected through a potting material that maintains each element in the targeted position.
For the standard read head design, used in industrial applications, this potting material fully encapsulates the MR sensors, the rigid part of the PCB and the magnets as illustrated in Fig. 10. The advantage of this design is that all sensitive parts are fully protected against contamination and allows the use of the reading heads in dusty environments.

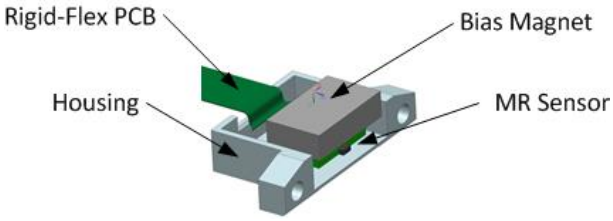

Figure 9. Read Head Key Elements

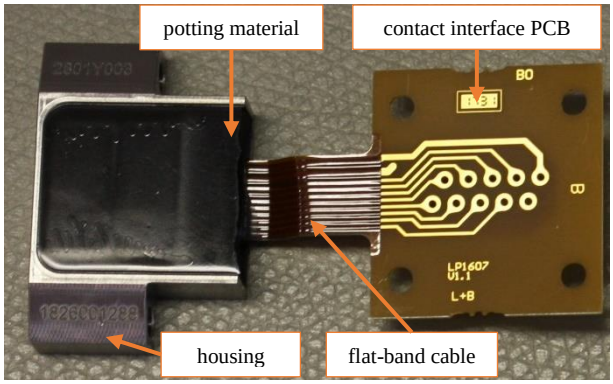

Figure 10. Read Head Industrial Design

3.2. Filter Wheel Assembly Challenges

The FWA is designed to survive the severe thermal condition in orbit for its lifetime of 7.5 years plus the harsh launch vibrations. The environmental loads for the FWA, including qualification margin, are reported in Tab. 1 where:

- The vibration loads are expressed as the Root Mean Square (RMS) of the spectrum.
- The shock is defined as Shock Response Spectrum (SRS).
- The radiation environment, Total Ionising Dose (TID) and Displacement Damage Equivalent Fluence (DDEF), is calculated considering 3 mm aluminium shielding and design margin of 2.

Table 1. FWA environmental loads

Thermal range	-40°C; +60°C
Vibration loads	RMS: x=22 g; y=22 g; z=13 g
Shock loads	SRS peak = 600 g
Revolutions	56.4 M
Radiation	TID = 40 krad(Si); DDEF = 4.6*10^10 10MeV p./cm^2

The GMR sensors are well suited for the application because they are nearly insensitive to radiation damage [5], they do not wear out since they are contactless and can sustain very high vibration and thermal loads.

4. ENHANCEMENT AGAINST ENVIRONMENTAL LOADS

4.1. Testing

A batch of read heads, manufactured according to the initial design was submitted to Lot Acceptance Tests (LAT) to verify the robustness of the reading heads against environmental loads.
LAT flow consists of various tests, executed on different lot from the initial batch, which are in general even more extreme than the qualification loads. For instance, the RMS vibration load was 99 g on all axes and up to 500 the thermal cycles, were performed between -55 °C and +100 °C. No change in the performances were observed due to bake-out, burn-in, vibration and irradiation but the thermal cycles highlighted some weaknesses: detachment of the potting material from the housing, see Fig. 11, and significant increase of resistance in some signal lines. In order to identify the root cause of the latter, several sensors have been submitted to micro sectioning, a destructive analysis consisting in grinding the device to capture high resolution microscopic pictures of the area of interest. The micro sectioning was done through the soldering joints of both sensor element chips on different lines: clear evidence of cracks, see Fig. 12, in the solder joints, for sensors submitted to thermal cycles, was found.

Figure 11. Read head failure due to thermal stresses

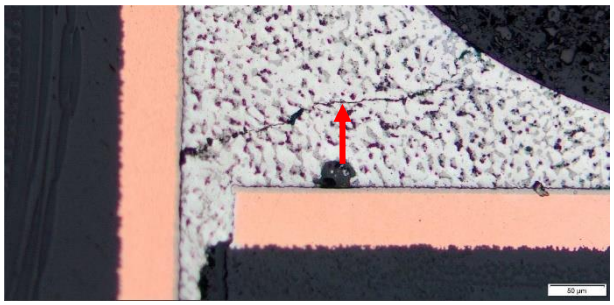

Figure 12. Micro section of the ground line solder joint: initial design

The coefficient of thermal expansion mismatch between the housing, the PCB and the potting material was found to be the root cause of the read head failures.
Another issue linked to thermal effects was identified during the TVAC tests performed at FWS level which showed that a reliable temperature measurement was not possible at cold temperatures. The cause for this issue was the thermal drift of the position sensor which was not compensated. Further analysis of the data showed a linear drift of the position sensor gain with respect to the temperature of the sensor itself: an example is shown in Fig. 14.

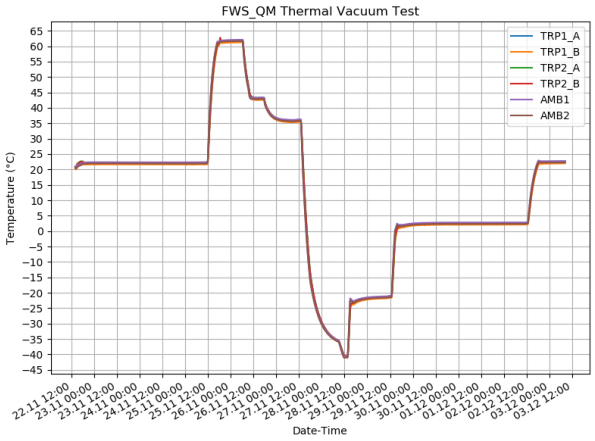

Figure 13. FWS first thermal cycle

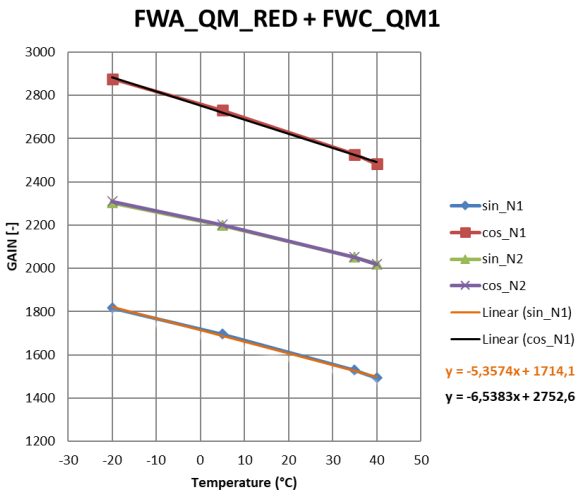

Figure 14. FWS gain thermal drift

The gradients of the linear regression for the different gains were ranging between 3.7 $°C^{-1}$ and 6.5 $°C^{-1}$. That is a relative change between 12 % and 18 % across the start-up range (-20 °C to +40 °C) of the FWA. Using a MATLAB model of the virtual wheel and the measured data from the FWS TVAC test it was possible to check the reliability of the position estimation at a given temperature. The PSSP model was run over thousands of sets of raw values, acquired during rotation, to estimate

position. The differences to the ideal position were computed and the results are reported in Fig. 15. The incorrect position measurements are characterised by a jump of ~4.7 ° with respect to the correct position. This is because each signal has a different temperature drift and the resulting minimum of the differential function, refer to chapter 2.4, then corresponds to a neighbouring tooth which is ~4.7 ° off. For the case presented in Fig. 15, 29.3 % of the 32227 evaluated points were computed wrongly. If the initial estimated position is wrong the FWD cannot be correctly positioned.
The position sensor thermal drift and the position sensor damages caused by CTE mismatch triggered an update of both the FWA reading head design and the FWC estimation algorithm.

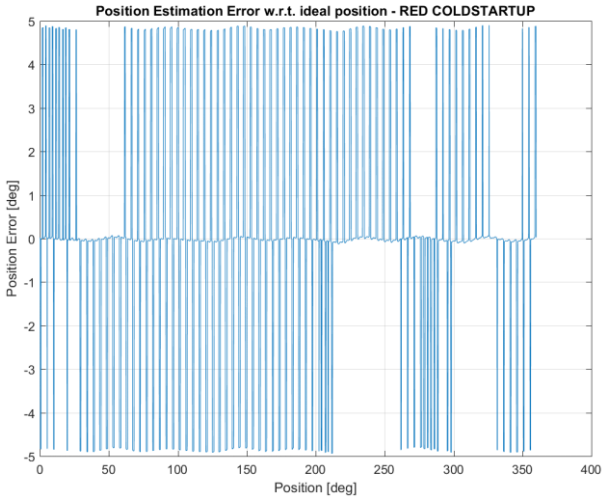

Figure 15. Position estimation reliability for FWS at cold start-up

4.2. Reading Head Design Optimisation

A modification of the read head elements mounting approach was deemed necessary to qualify the read head for use in space applications where it will be submitted to larger thermal variation than within its industrial application. With the root cause identified as the CTE mismatch of the key elements of the read head, the new design included a new housing and a new method of connecting the PCB to the housing.
The read heads were then submitted again to LAT and qualification but, in this case, they didn't show any sign of damage or deterioration: no detachment of the reading head from the housing or sign of crack initiation on GMR carrier solder joints. All the micro-sectioning performed after the LAT are similar to the one reported in Fig. 16.

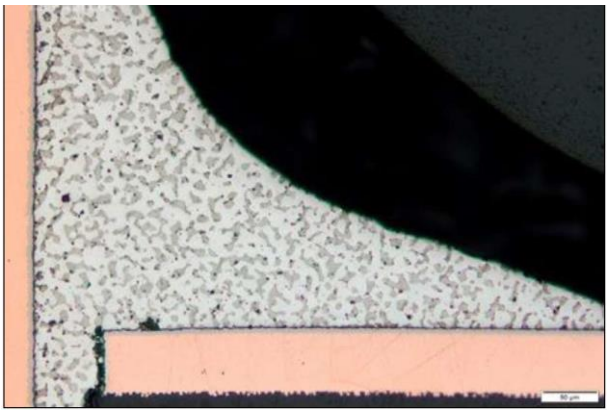

Figure 16. Micro section of the ground line solder joint: final design

4.3. Position Sensors Temperature Compensation

The results of TVAC testing during FWS test campaign showed insufficient reliability of the position estimation over the full temperature range, mostly visible at cold start-up. After detailed analyses, the selected method of position estimation was proven to be fully reliable only in temperature range of ±10 °C around the temperature used during calibration, in this case the ambient one. It was thus decided to keep the baseline of the estimation method but extending the generation of virtual wheel with a model for temperature drift. This extension is called Coefficient Temperature Compensation (CTC), see Fig. 4, and operates directly on the coefficients stored in the FWC memory.
From the measured data, see Fig. 14, it is clear that the amplitude of sensor signals is mainly affected by temperature drift and the relationship is almost perfectly linear (computed coefficients of determination for gain values $0.998 \leq R^2 \leq 0.999$). Since the FWS is equipped with temperature sensors located close to the position sensor, the information about the current temperature can be used to modify the coefficients before the virtual wheel is created thus avoiding additional hardware for the compensation.
The functionality of the compensation method was verified by simulation with the same input data used for reliability analysis, Fig. 15. After the introduction of the CTC, into the position estimation chain, the reliability over the full temperature range increased to 100% as shown in Fig. 17 and it was later on confirmed by the test campaign performed on the FWS Flight Model (FWS_FM).

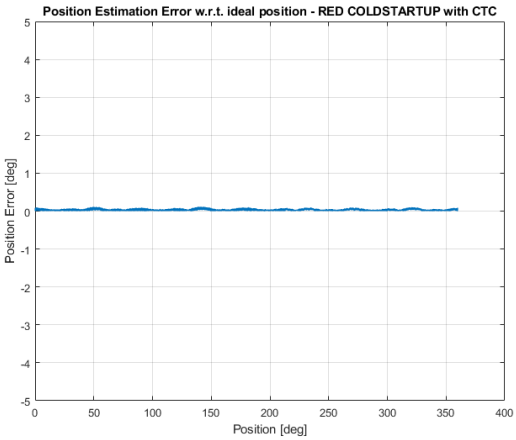

Figure 17. Position estimation reliability for FWS at cold start-up when using CTC

5. CONCLUSION

GMR contactless absolute position sensors are a good choice for space applications because they are nearly insensitive to radiation, compact, cost effective and able to sustain high vibration loads. Special attention should be taken when selecting an industrial design since they are not suited for the thermal range required by most of the space missions. Nevertheless, it has been demonstrated, by means of a meticulous test campaign conducted in the frame of Filter Wheel project, that a careful design of the read head can effectively increase its capability to sustain large temperature variations. If a proper read head design is paired with the robust position estimation method herein described, PSSP plus CTC, the absolute position can be reliably estimated over a very large temperature range with very high accuracy. This shows the readiness of the technology for space applications, as long as the resolution meets the requirements.

6. REFERENCES

1. N. Scheidegger, F. Vedovati, P. Frei, A. Lang, T. Knodel, M. Holland, M.J. Anderson (2019). Filter Wheel Assembly: a Long Life Space-Mechanism with Hard Mounted Bearings. ESMATS 2019.

2. Alistar, Kwan. (2011). Vernier scales and other early devices for precise measurement. American Journal of Physics. 2011(79), 368-373.

3. Zhang, Z., Dong, Y., Ni, F., Jin, M. & Liu, H. (2015). A Method for Measurement of Absolute Angular Position and Application in a Novel Electromagnetic Encoder Systém. Journal of Sensors, Volume 2015.

4. Nguyen, T.H., Nguyen, H.X., Tran, T.N., Park, J.W., Le, K.M., Nguyen, V.Q. & Jeon, J.W. (2021) An Effective Method to Improve the Accuracy of a Vernier-Type Absolute Magnetic Encoder. IEEE Transactions on Industrial Electronics, 68(8), 7330-7340.

5. Olfert J., Luloff B., MacDonald D., Lumsden R. (2015). On-line Irradiation Testing of a Giant Magneto-Resistive (GMR) Sensor. Canadian Nuclear Laboratories, Chalk River, ON K0J 1J0, Canada.